Developmental Biology **209,** 254–267 (1999)
Article ID dbio.1999.9253, available online at http://www.idealibrary.com on IDEAL®

Defective Vascularization of HIF-1α-Null Embryos Is Not Associated with VEGF Deficiency but with Mesenchymal Cell Death

Lori E. Kotch,[1] Narayan V. Iyer,[1] Erik Laughner, and Gregg L. Semenza[2]

Institute of Genetic Medicine and Department of Pediatrics and Department of Medicine, Johns Hopkins University School of Medicine, Baltimore, Maryland 21287-3914

Hypoxia-inducible factor 1 (HIF-1) is a dimeric transcription factor composed of HIF-1α and HIF-1β subunits that plays an essential role in mammalian O_2 homeostasis. In *Hif1a*$^{-/-}$ knockout mice, complete deficiency of HIF-1α resulted in cardiac and vascular malformations and embryonic lethality at E10.5. Between E8.75 and E9.25 striking vascular regression and abnormal remodeling occurred in the cephalic region concomitant with marked mesenchymal cell death. Similar vascular defects were observed in HIF-1α- and VEGF-deficient embryos and VEGF mRNA expression was not induced by hypoxia in *Hif1a*$^{-/-}$ embryonic stem cells. Surprisingly, *Hif1a*$^{-/-}$ embryos demonstrated increased VEGF mRNA expression compared to wild-type embryos. In tissue culture cells, VEGF mRNA expression was induced by glucose deprivation independent of HIF-1α, providing a mechanism for increased VEGF mRNA expression in *Hif1a*$^{-/-}$ embryos, in which absence of adequate tissue perfusion resulted in both O_2 and glucose deprivation. Rather than being associated with VEGF deficiency, the vascular defects in *Hif1a*$^{-/-}$ embryos were spatially correlated with cell death, the onset of which preceded vascular regression.

INTRODUCTION

The first functioning physiological system in mammalian embryogenesis is the circulatory system which ensures that every cell will receive adequate O_2 and glucose to meet its metabolic requirements. Development of the hematopoietic and cardiovascular systems initiates as the size of the embryo increases such that O_2 and glucose can no longer be provided to all cells by diffusion alone, suggesting that physiologic stimuli may play an important role in embryogenesis.

Hypoxia-inducible factor 1 (HIF-1) is a transcription factor that plays an essential role in O_2 homeostasis (Iyer *et al.*, 1998; Ryan *et al.*, 1998; Semenza and Wang, 1992; Wang *et al.*, 1995). HIF-1 is composed of HIF-1α and HIF-1β subunits (Wang *et al.*, 1995; Wang and Semenza, 1995). HIF-1β, which was previously identified as the aryl hydrocarbon receptor nuclear translocator (ARNT), is a common subunit for several members of the bHLH-PAS family of transcription factors in addition to HIF-1α (reviewed by Semenza, 1998). Whereas HIF-1β is expressed constitutively and in excess, HIF-1α is expressed at relatively low levels in most cell types under nonhypoxic conditions (Semenza *et al.*, 1996; Wang *et al.*, 1995; Yu *et al.*, 1998). As O_2 concentration decreases, the steady-state levels of HIF-1α protein increase exponentially and lead to the formation of increased amounts of biologically active HIF-1 (Jiang *et al.*, 1996; Semenza *et al.*, 1996; Yu *et al.*, 1998). The transcription of a large battery of genes is activated by HIF-1 under hypoxic conditions, including those encoding erythropoietin (EPO) and vascular endothelial growth factor (VEGF), the primary regulators of erythropoiesis and angiogenesis, respectively (reviewed by Semenza, 1998). Analysis of HIF-1α- or HIF-1β-deficient embryonic stem (ES) cells revealed absence of the normal induction of VEGF mRNA expression in response to hypoxia (Carmeliet *et al.*, 1998; Iyer *et al.*, 1998; Maltepe *et al.*, 1998; Ryan *et al.*, 1998). In addition, HIF-1α deficiency was associated with decreased expression of at least 13 different genes encoding glucose transporters and glycolytic enzymes (Iyer *et al.*, 1998). HIF-1 thus mediates increased O_2

[1] These authors contributed equally to this work.

[2] To whom correspondence should be addressed at Johns Hopkins Hospital, CMSC-1004, 600 North Wolfe St., Baltimore, MD 21287-3914. Fax: 410-955-0484. E-mail: gsemenza@jhmi.edu.

0012-1606/99 $30.00

delivery to cells (via EPO and VEGF) as well as adaptation to decreased O_2 availability (via glycolysis).

Mouse embryos homozygous for a null mutation in the *Hif1a* gene that resulted in complete HIF-1α deficiency developed normally until midgestation. Embryonic development arrested by E9.0 and the mice died by E10.5 (Iyer *et al.*, 1998; Ryan *et al.*, 1998). Analysis by light microscopy revealed that the gross morphology and vascular development of *Hif1a*$^{-/-}$ and *Hif1a*$^{+/+}$ embryos were indistinguishable at E8.5–E8.75 but by E9.25 there was a marked regression of vessels, especially in the cephalic region, and their replacement by a smaller number of abnormally enlarged vessels (Iyer *et al.*, 1998). Concomitant with the disruption of vascular development, massive cell death was observed within the cephalic mesenchyme. Cardiac development was also abnormal in *Hif1a*$^{-/-}$ embryos with hyperplasia of the presumptive myocardium that resulted in obliteration of the chamber lumens (Iyer *et al.*, 1998). HIF-1α protein expression in *Hif1a*$^{+/+}$ embryos increased between E8.5 and E9.5, the time at which malformations became apparent in *Hif1a*$^{-/-}$ embryos, which expressed no HIF-1α protein (Iyer *et al.*, 1998).

These data suggested at least two possible mechanisms for the vascular defects observed in *Hif1a*$^{-/-}$ embryos. First, deficiency of VEGF, either due to lack of HIF-1 expression or due to the loss of VEGF-producing mesenchymal cells, could be responsible since the vascular defects were remarkably similar to those observed in embryos heterozygous or homozygous for a knockout allele at the *Vegf* locus (Carmeliet *et al.*, 1996; Ferrara *et al.*, 1996). Second, the death of vascular endothelial and/or supporting mesenchymal cells might be the primary cause of the vascular defects. In this study, we utilized embryological and molecular biological techniques to test these hypotheses.

MATERIALS AND METHODS

Timed Matings and Genotype Analysis

For timed matings, *Hif1a*$^{+/-}$ or *Hif1a*$^{+/+}$ mice that were at least 8 weeks old were mated and female mice were examined for the presence of vaginal plugs twice daily. Depending on whether vaginal plugs were detected in the morning (10:30 AM) or evening (6:30 PM), the gestational age of the embryos at 12:00 noon was considered to be E0.5 or E0.0, respectively. Pregnant females were sacrificed by cervical dislocation, the abdominal cavity and uterus were opened, and viable embryos were harvested for study. Somite pairs were counted and rotation along the craniocaudal axis was scored as 100, 75, 50, 25, and 0% in all embryos. Genotype analysis of the embryos was performed by PCR as described (Iyer *et al.*, 1998).

Scanning Electron Microscopy (SEM)

Eighteen E8.5 or E9.75 *Hif1a*$^{-/-}$ and 6 stage-matched *Hif1a*$^{+/+}$ embryos were collected and processed for analysis by SEM as previously described (Kotch *et al.*, 1995). The specimens were fixed in 2.5% glutaraldehyde, rinsed in Sorenson's phosphate buffer (pH 7.3), postfixed in 2% osmium tetroxide, rinsed, and dehydrated through a graded alcohol series. They were then critical point dried from CO_2 and mounted on aluminum stubs. Specimens were coated with gold palladium and examined at 15 kV with a JEOL scanning electron microscope.

Nile Blue Sulfate (NBS) Staining

At E8.5, E9.25, and E9.75, at least six *Hif1a*$^{-/-}$ and *Hif1a*$^{+/+}$ embryos each were stained with NBS (Kotch *et al.*, 1995). All extraembryonic membranes were removed, and the embryos were staged by somite number. The yolk sacs (or portions thereof) were collected in separate vials for genotype determination by PCR analysis (Iyer *et al.*, 1998). Vital embryos were incubated in a 1:50,000 solution of NBS in lactated Ringer's solution at 37°C for 30 min. The stained specimens were then rinsed in Ringer's solution and photographed using a Nikon photomicroscope.

Histology

Five E9.75–E10.0 *Hif1a*$^{-/-}$ and *Hif1a*$^{+/+}$ embryos, each from a different pregnancy, were examined histologically. Embryos were fixed in Bouin's solution, rinsed in 70% alcohol, dehydrated through a graded alcohol series, and embedded using a Polysciences JB4 kit. The embedded tissue was sectioned at 4 μm on a Sorvall microtome and stained in methylene blue–acid fuchsin for 15 min at pH 4.0. The sections were examined using a Nikon photomicroscope.

RNA Blot Hybridization

Embryos were lysed in guanidine isothiocyanate and total RNA was isolated by phenol–chloroform extraction (Chomczynski and Sacchi, 1987). Aliquots of RNA were fractionated by 2.2 M formaldehyde, 1.4% agarose gel electrophoresis and transferred to a Nytran membrane (Schleicher and Schuell). A full-length rat VEGF cDNA was used to generate a radiolabeled probe by random-primer synthesis using a commercial kit (Boehringer-Mannheim). Hybridization was performed in Quik-Hyb (Stratagene) at 67°C. Blots were washed in 0.1× SSC, 0.1% SDS at room temperature for 1 h, then at 55°C for 1 h, and subjected to autoradiography. Blots were stripped of radioactivity and hybridized with a ^{32}P-labeled oligonucleotide complementary to 18S rRNA (Semenza *et al.*, 1996).

Nuclear Extract Preparation for Immunoblot and Electrophoretic Mobility Shift Assays (EMSA)

Hep3B cells were grown to confluence on 150-mm plates in MEM with Earle's salts supplemented with 1 mM sodium pyruvate, nonessential amino acids, and 10% fetal bovine serum (Life Technologies, Inc.). The medium was changed to high-glucose DMEM supplemented with sodium pyruvate, L-glutamine, and cells were exposed to 1 or 20% O_2 for 6 h. At the same time, three plates were also changed to glucose-free DMEM supplemented with sodium pyruvate and incubated for 24, 48, or 72 h. Nuclear extracts were prepared as described (Wang and Semenza, 1995). For immunoblots, 40 μg of nuclear extracts was fractionated on a 7% SDS–polyacrylamide gel and transferred to a nitrocellulose membrane, which was incubated with anti-HIF-1α or anti-HIF-1β antibodies as previously described (Jiang *et al.*, 1996) followed by a 1:2000 dilution of goat anti-rabbit serum as a secondary antibody

for detection with ECL reagents (Amersham). Immunoblots were stripped and incubated with anti-human topoisomerase I antibody (TopoGEN) at 1:1000 dilution, followed by goat anti-human secondary antibody (Calbiochem) at 1:2000 dilution. For EMSA, 5 μg of the nuclear extracts was incubated with radiolabeled oligonucleotide probe W18, containing a HIF-1 binding site, and analyzed as described previously (Wang and Semenza, 1995).

Transient Transfection Assay

Reporter plasmids contained the *VEGF* promoter (nucleotides −2274 to +379 relative to the transcription start site) or SV40 promoter cloned 5′ to luciferase or β-galactosidase (β-gal) coding sequences, respectively (Forsythe *et al.*, 1996). Hep3B cells were electroporated with plasmid DNA using a Gene Pulser (Bio-Rad) at 260 V and 960 μF. Cells were allowed to recover for 24 h, the medium was changed, and cells were exposed to standard culture conditions (95% air and 5% CO_2) or hypoxia (1% O_2, 5% CO_2, and balance N_2) or transferred to glucose-free medium (glucose deprivation). Cells were harvested and resuspended in 0.25 M Tris–HCl (pH 8.0), and extracts were prepared by freeze–thaw lysis. β-Gal activity was determined by hydrolysis of *o*-nitrophenyl-β-D-galactopyranoside (Promega), using 25 μg of extract at 37°C for 1 h followed by spectrophotometric measurement at 420 nm. Luciferase activity was determined using 20 μg of cell extract and 100 μl of assay reagent (Promega). Light emission was measured for 15 s in a TD-2Oe luminometer (Turner).

RESULTS

Analysis of E9.75–E10.0 Hif1a$^{-/-}$ and Stage-Matched Hif1a$^{+/+}$ Embryos by SEM

To investigate the relationship between cell death, defective vascularization, and morphological abnormalities, we examined *Hif1a*$^{-/-}$ and *Hif1a*$^{+/+}$ embryos by SEM. Because E9.75–E10.0 *Hif1a*$^{-/-}$ embryos were considerably delayed in development, E8.75–E9.0 *Hif1a*$^{+/+}$ embryos were collected to allow matching by somite number. The *Hif1a*$^{+/+}$ embryos analyzed by SEM had a mean of 14.1 somites and no malformations were noted. Anterior neural tube closure was nearly complete, and the normal subdivisions of the neural tube into the fore-, mid-, and hindbrain were evident (Figs. 1A, 1C, and 1E). There were two or three branchial arches and grooves on the ventrolateral aspect of the face and neck (Fig. 1C), due to the expansion of mesenchymal cores derived from cranial mesoderm and neural crest cells deposited from the mid- and hindbrain regions of the neural folds. The maxillary and mandibular portions of the first branchial arch were apparent as a continuous structure (Fig. 1C).

E9.75–E10.0 *Hif1a*$^{-/-}$ embryos manifested multiple head and trunk malformations (Figs. 1B, 1D, and 1F). The most common anomalies identified were open neural tube defects (NTDs), prolapsed neural folds, and anomalous deep grooves at the neurosomatic junction (NSJ) which occurred concurrently in 89% of the *Hif1a*$^{-/-}$ embryos analyzed. These specimens also manifested abnormal depressions and flexures along the neural tube (Fig. 1B), especially in the mid- and forebrain. The observed surface defects were consistent with anomalous growth of neural tissue within the open neural tube and the profound loss of supporting mesenchymal cells that were previously demonstrated by histological analysis of *Hif1a*$^{-/-}$ embryos (Iyer *et al.*, 1998). A marked unilateral dilatation of the left neural fold associated with the mid- and hindbrain regions (Fig. 1F), which was previously identified in whole-mount embryo preparations by light microscopy (Iyer *et al.*, 1998), was apparent in 50% of the *Hif1a*$^{-/-}$ embryos with NTDs.

A malformation that was uniformly associated with NTDs was branchial arch dysmorphogenesis, in which the first arch was dysmorphic and successive arches were hypoplastic or absent. In all cases, the proximal portion of the first arch was formed, but was abnormal in morphology, and the distal portion of the arch was severely hypoplastic. In most cases (75%), an anomalous distinct furrow was present between the distal and proximal portions of the arch (Fig. 1D). Histologic analysis of transverse sections at the level of the first arch confirmed the discontinuity of distal and proximal portions of the arch (data not shown). Extrusion of neural tissue through the posterior neuropore was noted in 89% of the specimens examined (Fig. 1F). *Hif1a*$^{-/-}$ embryos attained a mean rotation score of 36% compared to 100% for the *Hif1a*$^{+/+}$ embryos. In many *Hif1a*$^{-/-}$ embryos the somites were morphologically abnormal and misaligned with respect to the midline (data not shown).

Pericardial effusion, which was previously demonstrated by whole-mount and histological analysis (Iyer *et al.*, 1998), was also detected by SEM in 56% of the *Hif1a*$^{-/-}$ embryos, as evidenced by embryos with a collapsed pericardial sac (Fig. 1B). In addition, careful dissection of the pericardium demonstrated an increased pericardial space (Fig. 1D). In three embryos with obvious pericardial effusion, the pericardial sac was removed to demonstrate that the enlargement involved only the pericardial sac and not the developing heart (Fig. 1D). Three mutant specimens were fractured transversely at the level of somites 16–18, and at the level of the atrium, in order to reveal the dorsal aorta. Blood cells were detected within both the dorsal aorta (Fig.

FIG. 1. Morphological analysis of E9.75 embryos by SEM. Frontal (A and B), lateral (C and D), and dorsal (E and F) views of stage-matched *Hif1a*$^{+/+}$ embryos (A, C, and E) and E9.75 *Hif1a*$^{-/-}$ embryos (B, D, and F) are shown. In B, the distended pericardium (PC) ruptured and collapsed during specimen preparation and, in D, it was partially dissected away to reveal the heart (H). In B, D, and F, the neural folds (NF) are open and, in F, the left neural fold is massively enlarged compared to the adjacent right neural fold (not labeled). BA1, first branchial arch; BA2, second branchial arch; NT, neural tissue which has extruded through the posterior neuropore; SE, surface ectoderm.

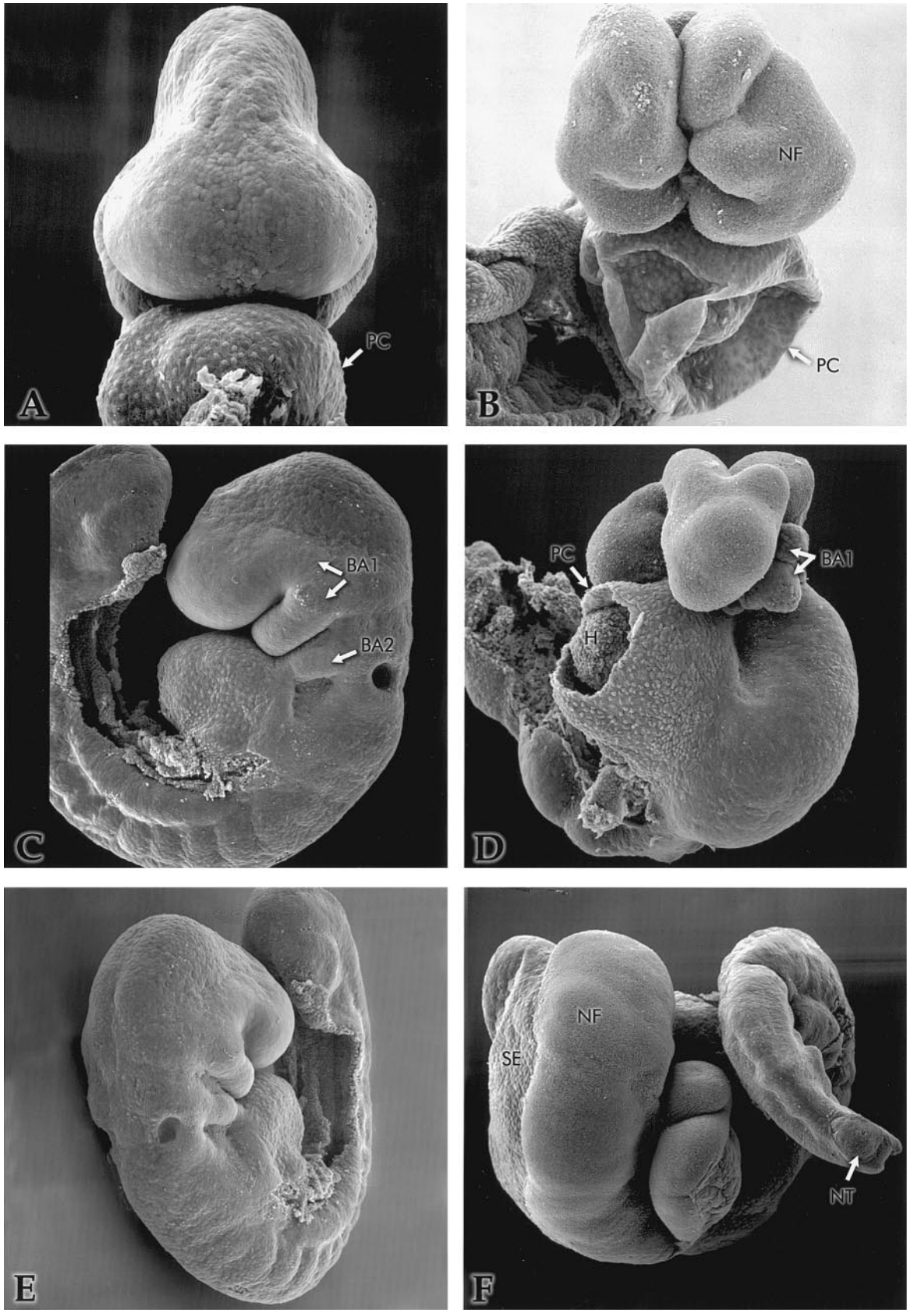

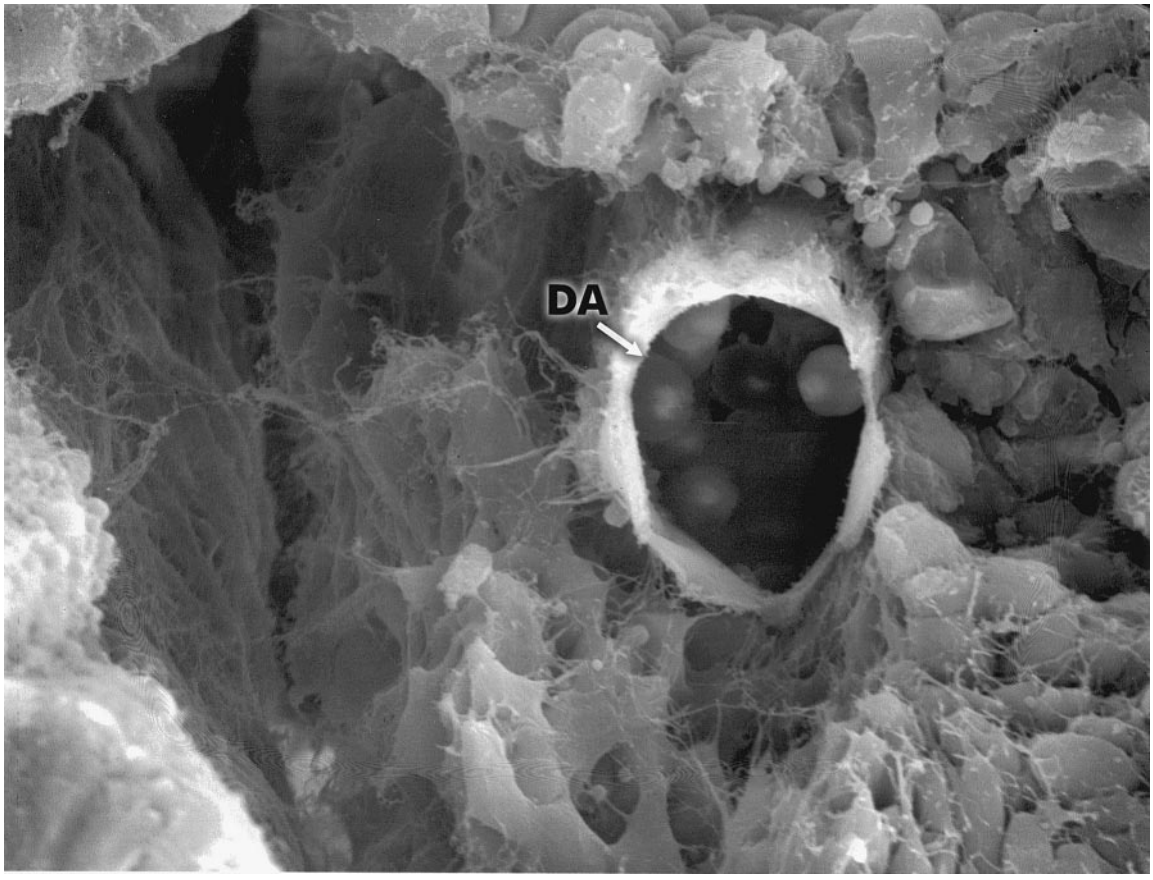

FIG. 2. Circulating blood cells in an E9.75 *Hif1a*$^{-/-}$ embryo. A section through the dorsal aorta (DA) reveals the presence of nucleated primitive blood cells within the lumen.

2) and the atrium (data not shown). Although these findings document the presence of red cells in *Hif1a*$^{-/-}$ embryos, it is not possible to determine from this analysis whether normal numbers of erythrocytes were present and whether they were efficiently circulating throughout the embryonic vasculature.

Analysis of E8.5–E8.75 Hif1a$^{-/-}$ *and Hif1a*$^{+/+}$ *Embryos by SEM*

Because E9.75–E10.0 *Hif1a*$^{-/-}$ embryos manifested multiple major malformations, embryos at an earlier stage of development were also studied in an attempt to determine the primary pathogenesis of these defects. In contrast to the developmental delay of the older embryos described above, *Hif1a*$^{-/-}$ embryos at E8.5–E8.75 had a mean of 12.2 somites compared to 11.0 somites for age-matched *Hif1a*$^{+/+}$ embryos and these two groups were therefore compared directly. The E8.5–E8.75 *Hif1a*$^{+/+}$ embryos analyzed by SEM had 8–16 somites. This stage is associated with the process of neurulation, and in all *Hif1a*$^{+/+}$ embryos the lateral margins of the thickened dorsal ectoderm, the neural plate, had become elevated to form the neural folds (Fig. 3A). In the more developmentally advanced *Hif1a*$^{+/+}$ embryos (13–16 somites) the neural folds had fused along the midline. The NSJ, a distinct line of transition from neural to surface ectoderm, was evident and served to demarcate the region from which neural crest cells arose and deposited inward to contribute to the underlying mesenchyme (Fig. 3A).

At this stage, the mouse embryo measures less than 1 mm along the craniocaudal axis, and by light microscopy the only difference between *Hif1a*$^{-/-}$ and *Hif1a*$^{+/+}$ embryos was a subtle prolapse of the lateral edges of the elevating neural folds (data not shown). By SEM, however, *Hif1a*$^{+/+}$ and *Hif1a*$^{-/-}$ embryos differed markedly in their cranial morphology. The neural folds of the latter were not normally elevated, especially along the lateral edges of the mesencephalon, and the NSJ within the mesencephalon appeared abnormally depressed, creating a deep groove (Fig. 3B). An excessive amount of cellular debris in the NSJ was apparent in several specimens. In addition to the dysmorphology associated with the lateral edge of the neural ectoderm, the medial aspects of the mesencephalic neural

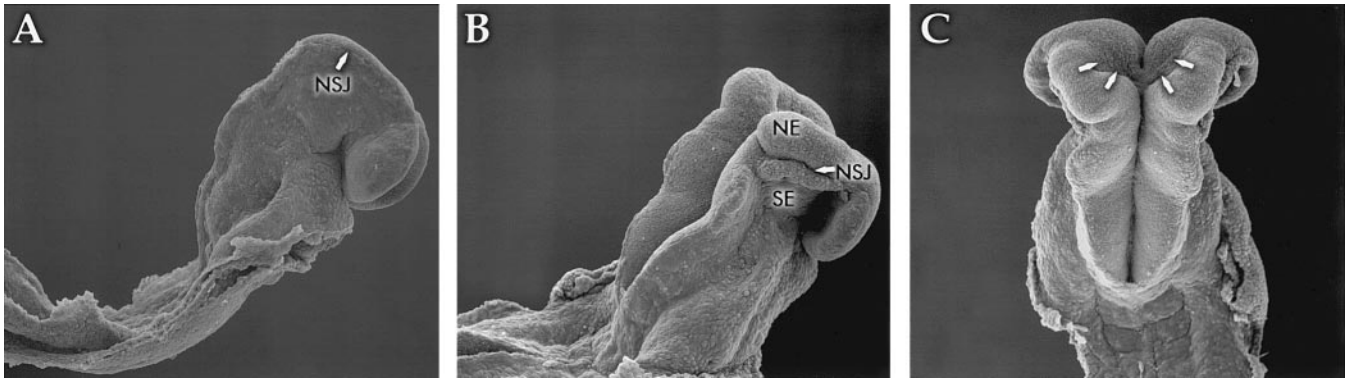

FIG. 3. Morphological analysis of E8.5–E8.75 embryos by SEM. Comparison of *Hif1a*$^{+/+}$ (A) and *Hif1a*$^{-/-}$ (B and C) seven-somite embryos. The neural folds are not properly elevated (B). Abnormal depressions are apparent within the neurosomatic junction (NSJ) at the interface between the neural ectoderm (NE) and surface ectoderm (SE). An enlarged gap is present between the medial portions of the opposing mesencephalic neural folds (arrows in C).

folds were reduced in thickness, resulting in an enlarged gap between the opposing neural folds along the midline (Fig. 3C). SEM thus demonstrated the consistent presence of morphological abnormalities of *Hif1a*$^{-/-}$ embryos as early as E8.5–E8.75, whereas no vascular abnormalities were detected at this stage of development (Iyer *et al.*, 1998).

Supravital Staining and Histology of Hif1a$^{-/-}$ and Hif1a$^{+/+}$ Embryos

Hif1a$^{-/-}$ and *Hif1a*$^{+/+}$ embryos at E8.5–E8.75, E9.25, and E9.75 were stained with the supravital dye NBS to comprehensively map patterns of cell death. In 50% of the *Hif1a*$^{-/-}$ embryos examined at E8.5–E8.75, an excessive amount of NBS staining was detected along the NSJ of the forebrain and midbrain (Fig. 4B) compared to *Hif1a*$^{+/+}$ embryos (Fig. 4A). Histological sections through the cranial end of the embryo revealed that in some specimens the mesenchymal compartments of the prosencephalic and mesencephalic regions contained significantly fewer cells than in *Hif1a*$^{+/+}$ embryos and confirmed that the regions showing excessive NBS uptake contained an increased number of dead or dying cells (data not shown). These results indicate that the abnormal depressions observed in *Hif1a*$^{-/-}$ embryos by SEM (Figs. 1B, 3B, and 3C) represented deficiencies of underlying tissue due to excessive cell death.

Compared to E8.5 embryos, supravital staining of E9.25 *Hif1a*$^{-/-}$ embryos showed more extensive cell death. All E9.25 *Hif1a*$^{-/-}$ embryos manifested a consistent pattern of cell death that was a more sensitive predictor of genotype than the presence or absence of morphological abnormalities by light microscopy. The NSJ, especially along the midbrain, demonstrated excessive NBS uptake in all specimens, again indicating that the NSJ defects visualized by SEM (Fig. 3B) were associated with excessive cell death.

At E9.75–E10.0 the predominant tissues containing excessive amounts of NBS stain were the neural tube and somites (80%) and the primitive streak (60%), a posterior midline ectodermal groove from which the embryonic mesoderm arises (Figs. 4D–4F). The first arch and neuroepithelium of the hindbrain demonstrated excessive cell death in 40% of the specimens. The neural tube contained dead cells along its entire length, but the location of cell death within the tube was dependent upon axial position within the embryo. Analysis of sections anterior to the heart revealed that cell death was confined to the alar plate, which is the distal region of the fusing neural folds (data not shown). In contrast, analysis of sections at the level of the heart revealed that cell death was localized to the midregion of the neural tube (Fig. 4F). Excessive cell death was apparent in the somitic mesoderm, especially at axial levels below the heart, as well as within the primitive streak (Fig. 4E). A particularly striking aspect of the *Hif1a*$^{-/-}$ embryos observed at this time point was the translucent appearance of the head region (Fig. 4D), which resulted from the extensive loss of mesenchymal cells 12–18 h earlier (Fig. 4B).

These results were confirmed by histological sectioning of the cranial region of E9.75–E10.0 *Hif1a*$^{-/-}$ embryos. A marked deficiency of cranial mesenchyme, in conjunction with excessive death within the remaining mesenchymal cell population, was observed in *Hif1a*$^{-/-}$ embryos compared to stage-matched *Hif1a*$^{+/+}$ embryos (Fig. 5). Abnormally enlarged endothelial-lined vascular structures occupied the vacant cephalic mesenchymal compartments of the *Hif1a*$^{-/-}$ embryos (Figs. 5B and 5D). In many specimens, the endothelium was markedly attenuated and discontinuous (Fig. 5D). The anomalous vasculature may have contributed to the dilatation of the neural folds demonstrated by SEM (Fig. 1F).

FIG. 4. Analysis of cell death. NBS demonstrated increased cell death (punctate dark blue staining) along the NSJ in an E8.5–E8.75 *Hif1a*$^{-/-}$ embryo (arrowheads in B) compared to a *Hif1a*$^{+/+}$ embryo (A). At E9.75–E10.0, anomalous acellular regions within the cephalic mesenchymal compartment of *Hif1a*$^{-/-}$ embryos were observed and the arrow in D indicates an area in which translucence of the head allows visualization of the dark background on which the embryo has been placed. The neural tube (arrowheads in D and F) and the primitive streak (within boxed area of D; arrowhead in E) of *Hif1a*$^{-/-}$ embryos manifested increased cell death compared to a stage-matched *Hif1a*$^{+/+}$ embryo (C; arrowheads indicate developmentally programmed cell death in the hindbrain rhombomeres). A transverse section at the level indicated (dashed line in D) demonstrates that cell death is localized to the midregion of the neural tube at this axial level (F). A histologic section at the same axial level also demonstrates excessive cell death within the midregion of the neural tube (inset in F).

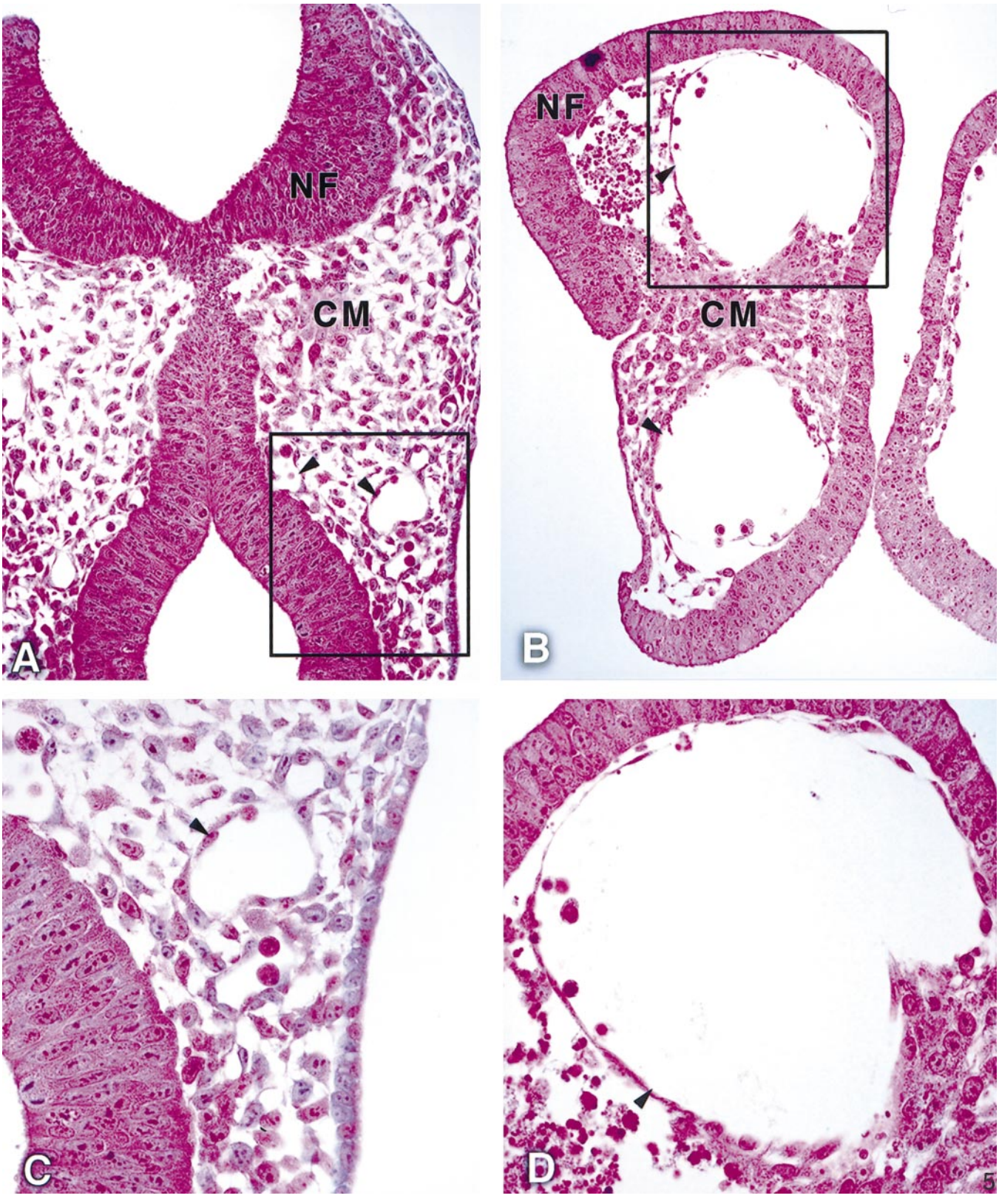

From these results the following conclusions can be drawn regarding the pattern of cell death in *Hif1a*$^{-/-}$ embryos: (i) Cell death involved multiple tissue types in a distinct temporospatial pattern, localizing in the cephalic region at earlier stages and extending more caudally at later stages. (ii) Certain cell populations (e.g., cephalic mesenchyme) and even certain subpopulations within a given tissue (e.g., neural tube) were particularly susceptible to cell death. (iii) The heart was notably resistant to cell death (data not shown), which accounted for the survival of *Hif1a*$^{-/-}$ embryos (as defined by the presence of cardiac contractions) until E10.5 despite extensive cell death elsewhere throughout the embryo.

Analysis of VEGF mRNA Expression in Mouse Embryos

To determine whether the striking developmental defects observed in *Hif1a*$^{-/-}$ embryos were associated with deficient expression of VEGF mRNA, blot hybridization was performed using total RNA extracted from *Hif1a*$^{-/-}$ and *Hif1a*$^{+/+}$ embryos. Several different comparisons were made in order to control for the marked developmental arrest of *Hif1a*$^{-/-}$ embryos. In the first case, 10 μg of total RNA from E9.5 *Hif1a*$^{-/-}$ embryos was analyzed in parallel with equal amounts of RNA from E8.75, E9.0, and E9.5 *Hif1a*$^{+/+}$ embryos. Surprisingly, *Hif1a*$^{-/-}$ embryos expressed higher levels of VEGF mRNA per microgram of total RNA than *Hif1a*$^{+/+}$ embryos, regardless of gestational age (Fig. 6A). Because *Hif1a*$^{-/-}$ embryos were much smaller than *Hif1a*$^{+/+}$ embryos and contained less RNA, the amount of RNA recovered per embryo was calculated and constant embryo equivalents of RNA were analyzed. *Hif1a*$^{-/-}$ embryos also expressed higher levels of VEGF mRNA per embryo than *Hif1a*$^{+/+}$ embryos, regardless of gestational age (Fig. 6B). Finally, 15-μg aliquots of total RNA extracted from *Hif1a*$^{+/+}$, *Hif1a*$^{+/-}$, and *Hif1a*$^{-/-}$ littermates at E9.25 were analyzed. Again, *Hif1a*$^{-/-}$ embryos demonstrated the highest levels of VEGF mRNA expression (Fig. 6C).

Analysis of Tissue Culture Cells Subjected to Hypoxia or Glucose Deprivation

In cultured cells, VEGF mRNA expression can be induced by either hypoxia or glucose deprivation (Shweiki *et al.*, 1992; Stein *et al.*, 1995). Hypoxia-induced transcriptional activation of the human *VEGF* gene is mediated by binding of HIF-1 at a site 1 kb 5′ to the transcription initiation site (Forsythe *et al.*, 1996; Liu *et al.*, 1995). We have previously demonstrated that in HIF-1α-deficient ES cells VEGF mRNA is induced by glucose deprivation but not by hypoxia, indicating that HIF-1 specifically mediates transcriptional responses to hypoxia (Iyer *et al.*, 1998). However, analysis of gene expression in ES cells lacking expression of HIF-1α or HIF-1β by several other laboratories suggested that HIF-1 may play a role in response to glucose deprivation (Carmeliet *et al.*, 1998; Maltepe *et al.*, 1997; Ryan *et al.*, 1998). To explore this issue in greater detail, we analyzed expression of VEGF mRNA in human Hep3B cells under standard culture conditions (20% O_2 and 25 mM glucose; Fig. 7, lane 1) or under conditions of hypoxia (lane 2) or glucose deprivation (lanes 3–5). VEGF mRNA expression was induced in cells subjected to 1% O_2 for 6 h (lane 2) or glucose deprivation for 48–72 h (lanes 4 and 5). Nuclear extracts were prepared from duplicate plates for analysis of HIF-1α and HIF-1β protein expression. HIF-1α expression and HIF-1 DNA-binding activity were induced in response to hypoxia (lane 2) but not under conditions of glucose deprivation identical to those which induced VEGF mRNA expression (lanes 4 and 5). Analysis of topoisomerase I expression demonstrated that all samples contained equal amounts of protein.

These results indicated that the induction of VEGF mRNA in glucose-deprived cells was not mediated by HIF-1, a conclusion which is consistent with the observed induction of VEGF mRNA expression in glucose-deprived *Hif1a*$^{-/-}$ ES cells (Iyer *et al.*, 1998). To investigate whether the induction of VEGF mRNA in glucose-deprived cells involved transcriptional activation of the *VEGF* gene, Hep3B cells were transfected with a reporter gene in which a 2.7-kb DNA fragment encompassing the human *VEGF* gene promoter was cloned 5′ to luciferase coding sequences. Compared to control transfected cells, the relative luciferase activity was induced 8.0-fold in Hep3B cells exposed to 1% O_2 for 24 h (Fig. 8), which was in agreement with previous studies (Forsythe *et al.*, 1996). In contrast, cells deprived of glucose for 72 h showed no induction of reporter gene transcription. Glucose deprivation for 24 or 48 h also failed to induce expression of the *VEGF* reporter (data not shown). Cells subjected to both glucose deprivation and hypoxia for 72 h showed only a 4.3-fold induction of luciferase activity, compared to the 8.0-fold induction that was observed in cells subjected to hypoxia for 24 h in the presence of glucose.

FIG. 5. Histological analysis. Transverse sections through the cranial region of stage-matched *Hif1a*$^{+/+}$ (A, C) and E9.75–E10.0 *Hif1a*$^{-/-}$ (B, D) embryos are shown. Abnormally enlarged vascular structures in a *Hif1a*$^{-/-}$ embryo (arrowheads in B) can be compared with the normal vasculature in a *Hif1a*$^{+/+}$ embryo (arrowheads in A). CM, cephalic mesenchyme; NF, neural fold. Magnification: 20× (A, B), 40× (C, D).

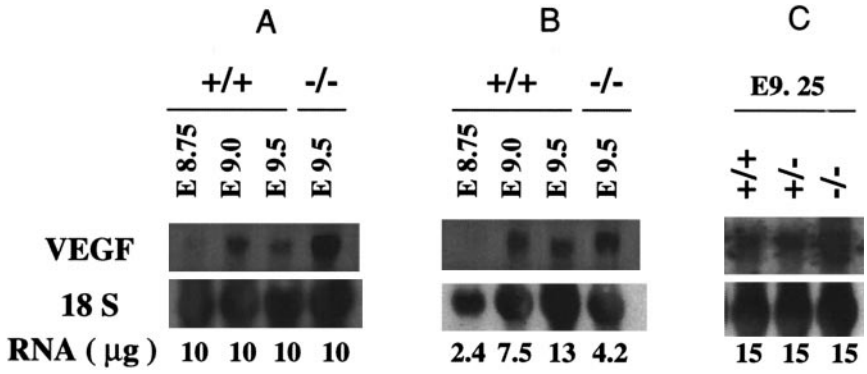

FIG. 6. VEGF mRNA expression in mouse embryos. Total RNA extracted from mouse embryos of indicated genotype and gestational age were analyzed by Northern blot hybridization using a VEGF cDNA probe. Following autoradiography, blots were stripped of radioactivity and hybridized with an oligonucleotide probe for 18S rRNA. (A) Analysis of 10-μg aliquots of total RNA from *Hif1a*$^{+/+}$ and *Hif1a*$^{-/-}$ embryos. (B) Analysis of single embryo equivalents of total RNA. Amount of RNA loaded per lane (in μg) is indicated at bottom. (C) Analysis of 15-μg aliquots of total RNA from *Hif1a*$^{+/+}$, *Hif1a*$^{+/-}$, and *Hif1a*$^{-/-}$ littermates at E9.25.

DISCUSSION

Cell Death Precedes Vascular Regression in Hif1a$^{-/-}$ Embryos

We previously performed whole-mount PECAM-1 immunohistochemistry to visualize vascular endothelial cells in *Hif1a*$^{-/-}$ and *Hif1a*$^{+/+}$ embryos. This analysis demonstrated that vascular development appeared normal in *Hif1a*$^{-/-}$ embryos at E8.5–E8.75 but subsequently underwent a dramatic regression in the cephalic and branchial regions that was associated with the appearance of multiple major malformations and developmental arrest (Iyer *et al.*, 1998). We have now demonstrated that prior to the onset of vascular or gross morphological defects *Hif1a*$^{-/-}$ embryos manifested extensive cell death both at the NSJ (Figs. 3 and 4) and in the cephalic mesenchyme (Iyer *et al.*, 1998). Neural crest cells, which emigrate from the neural tube at the NSJ to populate the cephalic mesenchyme, are highly sensitive to a variety of teratogens including hypoxia (Sulik *et al.*, 1988), perhaps because apoptosis is an essential aspect of their normal developmental program (Lumsden *et al.*, 1991; see Fig. 4C). There was no evidence of a circulatory defect in *Hif1a*$^{-/-}$ embryos at E8.5–E8.75 suggesting that in the absence of HIF-1α neural crest cells may be unable to survive the physiologic hypoxia associated with this stage of embryogenesis. A large body of data indicates that neural crest cells make an essential contribution to the developing circulatory system (Bergwerff *et al.*, 1998; Fukiishi and Morriss-Kay, 1992; Le Lievre and Le Douarin, 1975). In particular, neural crest cells are required not for the formation, but rather for the persistence of aortic arch arteries (Waldo *et al.*, 1996). Thus, the loss of neural crest cells at E8.5–E8.75 may contribute to vascular regression at E9.25–E9.75.

VEGF mRNA Induction by Glucose Deprivation Is Not Mediated by HIF-1

We previously demonstrated induction of VEGF mRNA expression in *Hif1a*$^{+/+}$ ES cells subjected to hypoxia or glucose deprivation, whereas *Hif1a*$^{-/-}$ ES cells responded to glucose deprivation but not to hypoxia (Iyer *et al.*, 1998). We have now demonstrated that conditions of glucose deprivation that result in the induction of VEGF mRNA expression in Hep3B cells do not result in the induction of HIF-1α protein, HIF-1 DNA-binding activity, or expression of a reporter gene containing *VEGF* promoter sequences that mediate basal and hypoxia-induced transcription. These results indicate that either the induction of VEGF mRNA expression in glucose-deprived Hep3B cells is not mediated at the transcriptional level or the sequences mediating transcriptional activation are located outside the promoter sequences present within the reporter gene. Previous studies in tissue culture cells have demonstrated that hypoxia induces increased *VEGF* transcription as well as increased stability of VEGF mRNA (Ikeda *et al.*, 1995; Levy *et al.*, 1995, 1996; Stein *et al.*, 1995). Increased stability of VEGF mRNA in glucose-deprived cells has also been demonstrated (Stein *et al.*, 1995), but effects on transcription have not been investigated. It is therefore possible that the induction of VEGF mRNA in response to glucose deprivation occurs primarily via a posttranscriptional mechanism. Several other laboratories have suggested that HIF-1 may mediate changes in gene expression associated with glucose deprivation, based upon their analysis of *Arnt*$^{-/-}$ or *Hif1a*$^{-/-}$ ES cells. We attribute this difference in interpretation to the following potential factors: First, ARNT (HIF-1β) can dimerize with bHLH-PAS proteins other than HIF-1α and therefore the effect of ARNT deficiency on responses to glucose deprivation (Maltepe *et al.*, 1997) may occur inde-

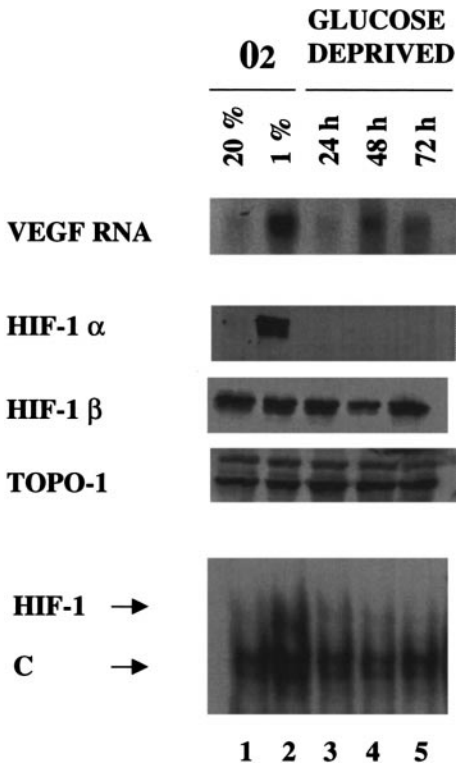

FIG. 7. Analysis of VEGF mRNA and HIF-1 expression in glucose-deprived Hep3B cells. Hep3B cells were exposed to standard culture conditions (20% O_2 and 25 mM glucose; lane 1), hypoxia (1% O_2 and 25 mM glucose) for 6 h (lane 2), or glucose deprivation (20% O_2 and 0 mM glucose) for 24–72 h (lanes 3–5). Total RNA was isolated for blot hybridization analysis of VEGF mRNA. Nuclear extracts were prepared from duplicate plates for immunoblot assays using antibodies against HIF-1α, HIF-1β, or topoisomerase I; and analysis of HIF-1 DNA-binding activity by EMSA, using a double-stranded oligonucleotide probe that binds both HIF-1 and constitutively expressed factors (C).

pendent of HIF-1. Second, the most striking effect of HIF-1α deficiency in ES cells was decreased basal VEGF mRNA expression (Carmeliet *et al.*, 1998; Iyer *et al.*, 1998). Responses to hypoxia were eliminated whereas in response to glucose deprivation a modest increase in VEGF mRNA expression was detected. Although the absolute level of VEGF mRNA was greatly reduced in glucose-deprived $Hif1a^{-/-}$ cells compared to $Hif1a^{+/+}$ cells, the fold induction was found to be comparable in these two cell types in the only study in which this was quantitated (Iyer *et al.*, 1998).

Pathogenesis of Vascular Defects in HIF-1α- and VEGF-Deficient Embryos

VEGF-deficient embryos were shown to have abnormally enlarged vascular structures at E9.5 whereas such structures were not described in E8.5 embryos (Carmeliet *et al.*, 1996). However, neither the stage at which these abnormal vessels arose nor their pathogenesis was described. We previously demonstrated that abnormally enlarged vessels strikingly similar to those in VEGF-deficient embryos were observed in HIF-1α-deficient embryos at E9.25 but not at E8.5–E8.75 (Iyer *et al.*, 1998). The similar pathology and the absence of hypoxia-induced VEGF mRNA expression in $Hif1a^{-/-}$ ES cells suggested that the vascular defects in $Hif1a^{-/-}$ embryos might be due to VEGF deficiency. However, in this paper we have demonstrated that in fact $Hif1a^{-/-}$ embryos have increased VEGF mRNA expression. By E9.25 $Hif1a^{-/-}$ embryos do not have a functioning circulatory system due to both cardiac and vascular malformations (Iyer *et al.*, 1998) and the absence of tissue perfusion would presumably result in severe O_2 and glucose deprivation. Since glucose deprivation induces VEGF mRNA expression independent of HIF-1α, it is likely that this stimulus is responsible for the high levels of VEGF mRNA in $Hif1a^{-/-}$ embryos. The extent to which reduced levels of O_2 and/or glucose serve as a stimulus for VEGF mRNA expression during the development of wild-type embryos remains to be established.

Rather than VEGF deficiency, the vascular defects of $Hif1a^{-/-}$ embryos were temporally and spatially correlated

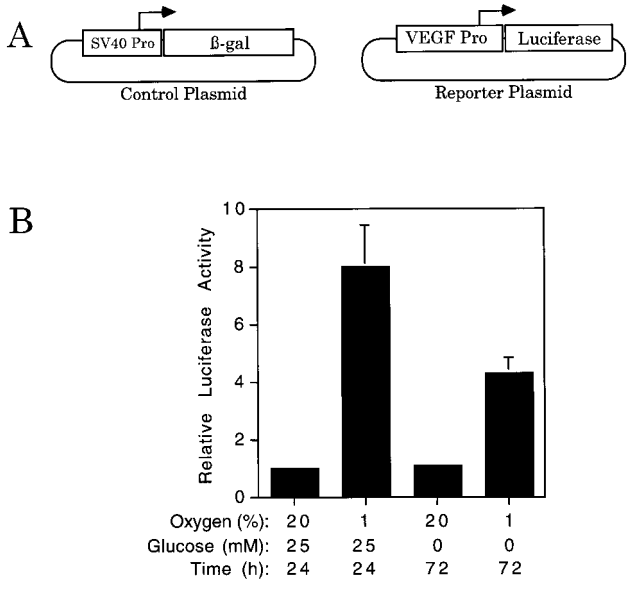

FIG. 8. Transient transfection assay. Hep3B cells were cotransfected with a reporter plasmid, containing the human *VEGF* gene promoter 5′ to luciferase coding sequences, and a control plasmid, containing a basal SV40 promoter 5′ to β-gal coding sequences (A). Transfected cells were exposed to 0 or 25 mM glucose and 1 or 20% O_2 for the indicated time (h). The ratio of luciferase:β-gal activity in cell lysates was determined and normalized to the result obtained from cells exposed to 25 mM glucose and 20% O_2 (relative luciferase activity). Data represent means ± SE from three plates of transfected cells (B).

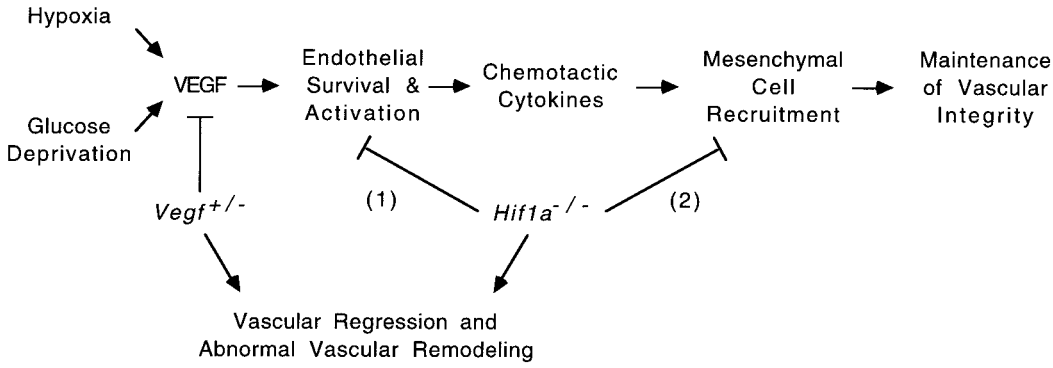

FIG. 9. Two models for the pathogenesis of vascular defects in HIF-1α-deficient mouse embryos. In model (1), endothelial cell death is directly responsible for vascular regression. In model (2), defective vascularization is due to failure to recruit supporting mesenchymal cells to the endothelium. These models are not mutually exclusive.

with cell death. The dramatic regression of blood vessels in the cephalic region indicates that extensive endothelial cell death occurred. Loss of endothelial cells could represent either a primary or secondary event in the pathogenesis of vascular regression in *Hif1a*$^{-/-}$ as well as *Vegf*$^{+/-}$ embryos. We propose two alternative models that are consistent with the data and are not mutually exclusive (Fig. 9).

Model (1): Endothelial cell death is a primary event. VEGF and HIF-1α deficiency may each result in a direct loss of endothelial viability. VEGF withdrawal has been shown to induce endothelial apoptosis in several experimental systems (Alon *et al.*, 1995; Benjamin and Keshet, 1997; Gerber *et al.*, 1998; Yuan *et al.*, 1996). VEGF deficiency may therefore result in endothelial death in *Vegf*$^{+/-}$ embryos. In *Hif1a*$^{-/-}$ embryos, the combined effects of ischemia and loss of metabolic adaptation to hypoxia may result in the death of endothelial as well as mesenchymal cells.

Model (2): Endothelial cell death is secondary to mesenchymal cell death. The formation of abnormally enlarged vessels suggests that active remodeling of the endothelium occurred. To account for this possibility, we propose that the loss of mesenchymal cell support of the vascular endothelium represented a critical event that induced vascular regression and remodeling. Extensive cell death was demonstrated in the NSJ (Figs. 3B and 4B) and cephalic mesenchyme (Figs. 4D and 5; Iyer *et al.*, 1998) of *Hif1a*$^{-/-}$ embryos. These locations suggest that the dying cells included pre- and postmigratory neural crest cells, respectively, which participate in the formation of most structures in the craniofacial region, including the supporting cells of the vasculature. Whereas recruitment of pericytes is not critical for the initial formation of endothelial tubes (vasculogenesis), subsequent vascular development is dependent upon proper endothelial–pericyte interactions (reviewed by Beck and D'Amore, 1997; Folkman and D'Amore, 1996). Previous studies have demonstrated that capillaries in the cephalic mesenchyme consist of endothelial cells coupled to pericytes via gap junctions as early as E9 of mouse development (Bauer *et al.*, 1993; Fujimoto, 1995), which coincides with the time at which vascular regression occurs in *Hif1a*$^{-/-}$ embryos (Iyer *et al.*, 1998). Experimental disruption of endothelial–pericyte associations in the developing rat retina resulted in dramatic vascular regression (Benjamin *et al.*, 1998). Pericyte recruitment is mediated in part through the secretion of platelet-derived growth factor-B, heparin-binding epidermal growth factor-like growth factor, and other chemotactic cytokines in response to VEGF binding to its receptors on vascular endothelial cells (Arkonac *et al.*, 1998; Benjamin *et al.*, 1998; Folkman and D'Amore, 1996; Lindahl *et al.*, 1997). Therefore, in VEGF-deficient embryos, supporting cells may not be recruited due to the lack of VEGF-induced cytokine production by endothelial cells. In HIF-1α-deficient embryos, the extensive mesenchymal cell death may include loss of pericytes and/or their progenitors.

Embryos deficient for the GTP-binding protein Gα_{13} developed enlarged vascular structures in the cephalic mesenchyme and Gα_{13} was shown to participate in ligand-induced cell motility (Offermanns *et al.*, 1997), suggesting that this signaling molecule may also be required for recruitment of mesenchymal cells to the endothelium. Further analysis of *Hif1a*$^{-/-}$ and *Vegf*$^{+/-}$ embryos, as well as the identification and investigation of similar vascular defects in other mutant mouse embryos, may provide additional insights into the molecular mechanisms regulating this critical phase of vascular development.

ACKNOWLEDGMENTS

We thank Dr. Kathleen Sulik for use of SEM facilities in the Department of Cell Biology and Anatomy, University of North Carolina at Chapel Hill. G.L.S. is an Established Investigator of the

American Heart Association and this work was supported by grants from the National Institutes of Health (R01-HL55338) and the American Heart Association National Center and Maryland Affiliate.

REFERENCES

Alon, T., Hemo, I., Itin, A., Pe'er, J., Stone, J., and Keshet, E. (1995). Vascular endothelial growth factor acts as a survival factor for newly formed retinal vessels and has implications for retinopathy of prematurity. *Nat. Med.* **1,** 1024–1028.

Arkonac, B. M., Foster, L. C., Sibinga, N. E. S., Patterson, C., Lai, K., Tsai, J.-C., Lee, M.-E., Perrella, M. A., and Haber, E. (1998). Vascular endothelial growth factor induces heparin-binding epidermal growth factor-like growth factor in vascular endothelial cells. *J. Biol. Chem.* **273,** 4400–4405.

Bauer, H. C., Bauer, H., Lametschwandtner, A., Amberger, A., Ruiz, P., and Steiner, M. (1993). Neovascularization and the appearance of morphological characteristics of the blood–brain barrier in the embryonic mouse central nervous system. *Dev. Brain Res.* **75,** 269–278.

Beck, L., Jr., and D'Amore, P. A. (1997). Vascular development: Cellular and molecular regulation. *FASEB J.* **11,** 365–373.

Benjamin, L. E., Hemo, I., and Keshet, E. (1998). A plasticity window for blood vessel remodeling is defined by pericyte coverage of the preformed endothelial network and is regulated by PDGF-B and VEGF. *Development* **125,** 1591–1598.

Benjamin, L. E., and Keshet, E. (1997). Conditional switching of vascular endothelial growth factor (VEGF) expression in tumors: Induction of endothelial cell shedding and regression of hemangioblastoma-like vessels by VEGF withdrawal. *Proc. Natl. Acad. Sci. USA* **94,** 8761–8766.

Bergwerff, M., Verberne, M. E., DeRuiter, M. C., Poelmann, R. E., and Gittenberger-de-Groot, A. C. (1998). Neural crest cell contribution to the developing circulatory system: Implications for vascular morphology? *Circ. Res.* **82,** 221–231.

Carmeliet, P., Dor, Y., Herbert, J.-M., Fukumura, D., Brusselmans, K., Dewerchin, M., Neeman, M., Bono, F., Abramovitch, R., Maxwell, P., Koch, C. J., Ratcliffe, P., Moons, L., Jain, R. K., Collen, D., and Keshet, E. (1998). Role of HIF-1α in hypoxia-mediated apoptosis, cell proliferation, and tumour angiogenesis. *Nature* **394,** 485–490.

Carmeliet, P., Ferreira, V., Breier, G., Pollefeyt, S., Kieckens, L., Gertsenstein, M., Fahrig, M., Vandenhoeck, A., Harpal, K., Eberhardt, C., Declercq, C., Pawling, J., Moons, L., Collen, D., Risau, W., and Nagy, A. (1996). Abnormal blood vessel development and lethality in embryos lacking a single VEGF allele. *Nature* **380,** 435–439.

Chomczynski, P., and Sacchi, N. (1987). Single-step method of RNA isolation by acid guanidinium thiocyanate–phenol–chloroform extraction. *Anal. Biochem.* **162,** 156–159.

Ferrara, N., Carver-Moore, K., Chen, H., Dowd, M., Lu, L., O'Shea, K. S., Powell-Braxton, L., Hillan, K. J., and Moore, M. W. (1996). Heterozygous embryonic lethality induced by targeted inactivation of the VEGF gene. *Nature* **380,** 439–442.

Folkman, J., and D'Amore, P. A. (1996). Blood vessel formation: What is its molecular basis? *Cell* **87,** 1153–1155.

Forsythe, J. A., Jiang, B.-H., Iyer, N. V., Agani, F., Leung, S. W., Koos, R. D., and Semenza, G. L. (1996). Activation of vascular endothelial growth factor gene transcription by hypoxia-inducible factor 1. *Mol. Cell. Biol.* **16,** 4604–4613.

Fujimoto, K. (1995). Pericyte–endothelial gap junctions in developing rat cerebral capillaries: A fine structural study. *Anat. Rec.* **242,** 562–565.

Fukuiishi, Y., and Morriss-Kay, G. M. (1992). Migration of cranial neural crest cells to the pharyngeal arches and heart in rat embryos. *Cell Tissue Res.* **268,** 1–8.

Gerber, H.-P., McMurtrey, A., Kowalski, J., Yan, M., Key, B. A., Dixit, V., and Ferrara, N. (1998). Vascular endothelial growth factor regulates endothelial cell survival through the phosphatidylinositol 3′-kinase/Akt signal transduction pathway: Requirement for Flk-1/KDR activation. *J. Biol. Chem.* **273,** 30336–30343.

Ikeda, E., Achen, M. G., Breier, G., and Risau, W. (1995). Hypoxia-induced transcriptional activation and increased mRNA stability of vascular endothelial growth factor in C6 glioma cells. *J. Biol. Chem.* **270,** 19761–19766.

Iyer, N. V., Kotch, L. E., Agani, F., Leung, S. W., Laughner, E., Wenger, R. H., Gassmann, M., Gearhart, J. D., Lawler, A. M., Yu, A. Y., and Semenza, G. L. (1998). Cellular and developmental control of O_2 homeostasis by hypoxia-inducible factor 1α. *Genes Dev.* **12,** 149–162.

Jiang, B.-H., Semenza, G. L., Bauer, C., and Marti, H. H. (1996). Hypoxia-inducible factor 1 levels vary exponentially over a physiologically relevant range of O_2 tension. *Am. J. Physiol.* **271,** C1172–C1180.

Kotch, L. E., Chen, S.-Y., and Sulik, K. K. (1995). Ethanol-induced teratogenesis: Free radical damage as a possible mechanism. *Teratology* **52,** 128–136.

Le Lievre, C. S., and Le Douarin, N. M. (1975). Mesenchymal derivatives of the neural crest: Analysis of chimaeric quail and chick embryos. *J. Embryol. Exp. Morphol.* **34,** 125–154.

Levy, A. P., Levy, N. S., and Goldberg, M. A. (1996). Post-transcriptional regulation of vascular endothelial growth factor by hypoxia. *J. Biol. Chem.* **271,** 2746–2753.

Levy, A. P., Levy, N. S., Wegner, S., and Goldberg, M. A. (1995). Transcriptional regulation of the rat vascular endothelial growth factor gene by hypoxia. *J. Biol. Chem.* **270,** 13333–13340.

Lindahl, P., Johansson, B. R., Leveen, P., and Betsholtz, C. (1997). Pericyte loss and microaneurysm formation in PDGF-B-deficient mice. *Science* **277,** 242–245.

Liu, Y., Cox, S. R., Morita, T., and Kourembanas, S. (1995). Hypoxia regulates vascular endothelial growth factor gene expression in endothelial cells. *Circ. Res.* **77,** 638–643.

Lumsden, A., Sprawson, N., and Graham, A. (1991). Segmental origin and migration of neural crest cells in the hindbrain region of the chick embryo. *Development* **113,** 1281–1291.

Maltepe, E., Schmidt, J. V., Baunoch, D., Bradfield, C. A., and Simon, M. C. (1997). Abnormal angiogenesis and responses to glucose and oxygen deprivation in mice lacking the protein ARNT. *Nature* **386,** 403–407.

Offermanns, S., Mancino, V., Revel, J.-P., and Simon, M. I. (1997). Vascular system defects and impaired cell chemokinesis as a result of Gα_{13} deficiency. *Science* **275,** 533–536.

Ryan, H. E., Lo, J., and Johnson, R. S. (1998). HIF-1α is required for solid tumor formation and embryonic vascularization. *EMBO J.* **17,** 3005–3015.

Semenza, G. L. (1998). Hypoxia-inducible factor 1: Master regulator of O_2 homeostasis. *Curr. Opin. Genet. Dev.* **8,** 588–594.

Semenza, G. L., Jiang, B.-H., Leung, S. W., Passantino, R., Concordet, J.-P., Maire, P., and Giallongo, A. (1996). Hypoxia

response elements in the aldolase A, enolase 1, and lactate dehydrogenase A gene promoters contain essential binding sites for hypoxia-inducible factor 1. *J. Biol. Chem*. **271,** 32529–32537.

Semenza, G. L., and Wang, G. L. (1992). A nuclear factor induced by hypoxia via *de novo* protein synthesis binds to the human erythropoietin gene enhancer at a site required for transcriptional activation. *Mol. Cell. Biol.* **12,** 5447–5454.

Shweiki, D., Itin, A., Soffer, D., and Keshet, E. (1992). Vascular endothelial growth factor induced by hypoxia may mediate hypoxia-initiated angiogenesis. *Nature* **359,** 843–845.

Stein, I., Neeman, M., Shweiki, D., Itin, A., and Keshet, E. (1995). Stabilization of vascular endothelial growth factor mRNA by hypoxia and hypoglycemia and coregulation with other ischemia-induced genes. *Mol. Cell. Biol.* **15,** 5363–5368.

Sulik, K. K., Cook, C. S., and Webster, W. S. (1988). Teratogens and craniofacial malformations: Relationships to cell death. *Development* **103**(Suppl.), 213–232.

Waldo, K. L., Kumiski, D., and Kirby, M. L. (1996). Cardiac neural crest is essential for the persistence rather than the formation of an arch artery. *Dev. Dyn.* **205,** 281–292.

Wang, G. L., Jiang, B.-H., Rue, E. A., and Semenza, G. L. (1995). Hypoxia-inducible factor 1 is a basic-helix-loop-helix-PAS heterodimer regulated by cellular O_2 tension. *Proc. Natl. Acad. Sci. USA* **92,** 5510–5514.

Wang, G. L., and Semenza, G. L. (1995). Purification and characterization of hypoxia-inducible factor 1. *J. Biol. Chem*. **270,** 1230–1237.

Yu, A. Y., Frid, M. G., Shimoda, L. A., Wiener, C. M., Stenmark, K., and Semenza, G. L. (1998). Temporal, spatial, and oxygen-regulated expression of hypoxia-inducible factor 1 in the lung. *Am. J. Physiol.* **275,** L818–L826.

Yuan, F., Chen, Y., Dellian, M., Safabakhsh, N., Ferrara, N., and Jain, R. K. (1996). Time-dependent vascular regression and permeability changes in established human tumor xenografts induced by an anti-vascular endothelial growth factor/vascular permeability factor antibody. *Proc. Natl. Acad. Sci. USA* **93,** 14765–14770.

Received for publication December 11, 1998
Revised February 18, 1999
Accepted February 18, 1999